SAND2022-11658C

16th International Conference on Greenhouse Gas Control Technologies, GHGT-16

23rd -27th October 2022, Lyon, France

Predictive digital twin of geologic CO_2 storage and plume evolution

Carlos A. S. Ferreira[a], Michal Stepien[a], Seyedbehzad Hosseinzadehsadati[a], Teeratorn Kadeethum[b], Hamidreza M. Nick[a,*]

[a]*Danish Offshore Technology Centre, Technical University of Denmark, Kgs. Lyngby, Denmark*
[b]*Sandia National Laboratories, Albuquerque, New Mexico, USA*

Abstract

The storage of CO_2 in geological formations is dependent on many uncertainties and poses as a challenge for the accurate description of the fluid flow pattern in the porous media where the carbon is stored. Conversely, accurate monitoring of the plume evolution is required for safe long-term operations, which is traditionally carried through the numerical simulation of the multiphase flow and plume motion. These simulations require solving large non-linear systems of equations, thus precluding real-time monitoring with such tools, in which we dynamically anticipate and/or mitigate the risks involved with the CO_2 storage. In this work, we propose the adaptation of continuous conditional generative adversarial networks (CCGAN) for a predictive digital twin of geologic CO_2 storage and plume motion. The proposed digital twin works in a sparse setting, meaning that it maps the sparsely available input data from three wells to the CO_2 saturation over the whole domain. The obtained results show that the digital twin enables fast prediction of the CO_2 plume with reasonable accuracy, by conferring a substantial reduction in the computational cost when compared to traditional numerical simulations.

Keywords: Monitoring tool; multimodal machine learning; GANs; reduced order modeling

1. Introduction

The sequestration storage of CO_2 into geological formations as a strategy for reducing atmospheric greenhouse gases requires accurate monitoring of CO_2 plumes for safe long-term storage [1, 2]. The standard approach to predicting CO_2 plume motion includes two main activities: (1) estimating the reservoir properties and phase saturation from seismic data [3-5] and (2) simulations of subsurface fluid flow in and plume movement [6-8]. This approach, however, may be impractical for rapid seismic monitoring in which ones dynamically anticipate or even mitigate risks associated with CO_2 injection [9-12]. This limitation reduces the engineer's ability to facilitate day-to-day reservoir management and ensure safe and smooth operations. Moreover, a curse of high dimensionality and limited resolving power of seismic monitoring cause extra uncertainty in the joint inversion of the seismic response and fluid flow parameter.

With improving computational power and emerging novel machine learning techniques, several works have applied models such as convolutional neural networks as surrogate models to mimic CO_2 plume evolution [13-17]. However, the more traditional reduced order models still fail to use in the actual field setting because it is difficult to

* Corresponding author. Email *address:* hamid@dtu.dk

parameterize heterogeneous material properties by a few parameters [18-20]. This limitation is one of the most challenging factors in reservoir management and surrogate modeling because subsurface physics commonly involves complex structures where the corresponding spatially distributed parameters (*e.g.*, permeability, porosity, saturation, or Young's modulus) can span several orders of magnitude and include discontinuous features.

To mitigate these issues, we illustrate a predictive digital twin that could model the CO_2 plume motion given uncertainties in the subsurface and operational parameters. These parameters include physical properties, geometric characteristics, or operating conditions. The fast and accurate estimation of plume position in real-time (during CO_2 storage operation and after injection) can assist evaluation of risks associated with CO_2 storage, *e.g.*, CO_2 leakage resulting from well integrity, non-sealed fractures in the caprock, or pressure build-up in the reservoir that could result in caprock hydraulic fracturing.

To achieve this, we employ continuous conditional generative adversarial networks (CCGAN) [21, 22] to efficiently parametrize the physical spatial heterogeneous properties and the operation conditions and measurements. Previous works have successfully shown the application of GANs [23] for predicting the solution of PDEs [22, 24, 25]. First, we carry multiple numerical simulations of two-phase flow for immiscible CO_2/brine in highly heterogeneous porous media with Petrel [26] and Eclipse 100 [27]. Following, we train a CCGAN-based digital twin with the average pressure, porosity, and injection rate at three wells as input and with the CO_2 saturation as output. Our results show that, despite the limited input data, a CCGAN-base digital twin can reasonably predict the plume evolution.

Nomenclature

$\boldsymbol{g}$	gravity
i	fluid phase notation
k	absolute permeability
$\boldsymbol{K}$	permeability tensor
k_r	relative permeability
ϕ	porosity
λ_x	correlation length in the direction x
λ_y	correlation length in the direction y
μ	fluid viscosity
p	pore pressure
q	source/sink term
S	fluid saturation
ρ	fluid density
$\boldsymbol{v}$	fluid flow velocity
σ	standard deviation

2. Methodology

In this work, we keep the fluid model as simple as possible, as we are concerned about the ability of our digital twin to make predictions of the CO_2 plume evolution with reasonable accuracy, given limited data from the wells. We model the process of carbon storage in a deep saline aquifer as isothermal and immiscible two-phase flow, *i.e.,* CO_2 and formation brine. Moreover, we simplify the model by assuming no capillary pressure and incompressible fluid flow.

Consequently, the governing equations describing displacement of the brine by injected CO_2 are Darcy's law and mass conservation, Eq. (1) and (2), consecutively:

$$\boldsymbol{v}_i + \frac{k_{ri}}{\mu_i}\boldsymbol{K}\cdot(\boldsymbol{\nabla} p_i - \rho_i \boldsymbol{g}) = 0, \qquad i = 1,2, \tag{1}$$

$$\frac{\partial}{\partial t}(\phi S_i \rho_i) + \boldsymbol{\nabla} \cdot (\rho_i \boldsymbol{v}_i) = q_i, \qquad i = 1,2, \tag{2}$$

where *i* symbolizes the phase, *i.e.,* CO_2 and brine, here denoted as phase 1 and 2, respectively.

Assuming no capillary pressure, we have $p_1 = p_2$, and thus combining Eq. (1) and (2) and noting that $S_1 + S_2 = 1$, yields

$$\frac{\partial}{\partial t}(\phi S_1 \rho_1) - \boldsymbol{\nabla} \cdot \left[\frac{\rho_1 k_{r1}}{\mu_1} \boldsymbol{K} \cdot (\boldsymbol{\nabla} p_1 - \rho_1 \boldsymbol{g})\right] = q_1, \tag{3}$$

$$\frac{\partial}{\partial t}(\phi (1 - S_1) \rho_2) - \boldsymbol{\nabla} \cdot \left[\frac{\rho_2 k_{r2}}{\mu_2} \boldsymbol{K} \cdot (\boldsymbol{\nabla} p_1 - \rho_2 \boldsymbol{g})\right] = q_2, \tag{4}$$

where Eq. (3) and (4) are mass conservation equations for CO_2 and formation brine, correspondingly.

There are two unknowns, S_1 and p_1, and we need a constitutive relationship for the relative permeability, that is $k_{ri} = k_{ri}(S_i)$. In this work, we assume a linear relationship between saturation and relative permeability, $k_{ri} = S_i$. The mathematical model given by Eq. (3) and (4) is solved using Eclipse 100 [27].

The geometry of our problem, along with the domain discretization, are defined in Petrel [26], in which we define the wells, their connectivity with the formation, and the material properties. When generating porosity and permeability fields, we consider homogeneous fields or heterogeneous fields using Gaussian distributions with varying standard deviation and correlation lengths in *x* and *y* directions. We choose the black-oil model composed of gas and water phases, that is CO_2 and brine, respectively, with constant density and viscosity. Subsequently, with given initial/boundary conditions, and the injection strategy, the model is numerically solved using Eclipse 100 [27].

Our digital twin is designed to process the data over a squared domain with a size of 128 × 128. Therefore, the results from the numerical simulations solved for the original domain must be mapped to the transformed domain with a size of 128 × 128. For that purpose, we employ a nearest-neighbor interpolation method, and an illustration of the mapping from one domain to another is shown in Fig. 1. From now on, all presented data is considered for the transformed domain, unless otherwise specified.

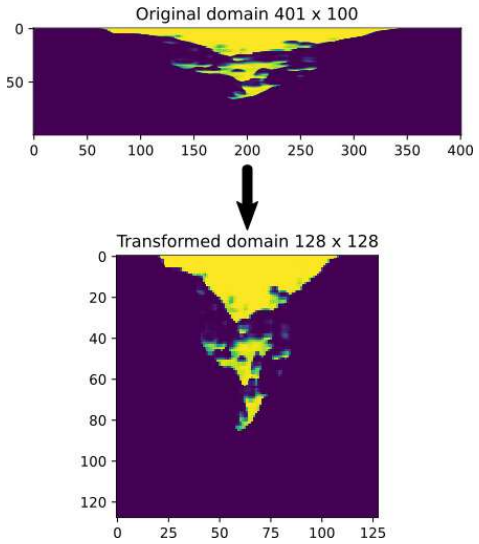

Fig. 1. Example of mapping the CO_2 saturation (plume) from an original domain with a size of 401 × 100, to the transformed domain with a size of 128 × 128.

Given the CO_2 injection rate, and the material properties estimations, we can simulate the plume movement with time, using the numerical framework outlined above. However, the uncertainty involved in estimating the material

properties requires a multiplicity of numerical simulations for history-matching of the measurements from the monitoring wells, which for real-time monitoring is unfeasible.

The proposed digital twin utilizes continuous conditional generative adversarial networks [21, 22] referred to as CCGAN in this paper, to predict the saturation distribution using the input data from the injection well and the two adjacent monitoring wells, with the aim of substantially reducing the computational cost, and allowing the set-up of a real-time monitoring tool.

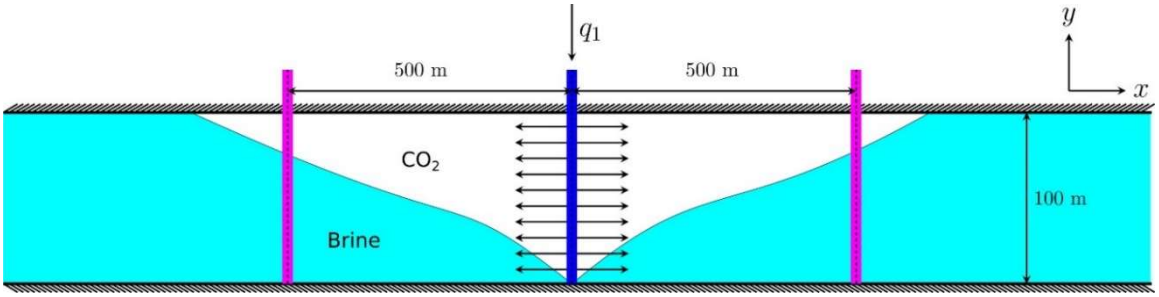

Fig. 2. Cross section of the formation, showing the position of the injection well and the two adjacent monitoring wells. We assume a constant rate injection of CO_2 in supercritical state through a vertical well in the centre (in blue). Two monitoring wells (in magenta) are located 500 m from the injection well.

3. Digital twin

The digital twin proposed in this work has the CO_2 saturation field as output, whereas the input is a combination of the data available only at the wells, in this case, average pressure, porosity and injection rate. We employ continuous conditional generative adversarial networks (CCGAN) for reduced order modelling [21, 22]. The CCGAN in this work has the same architecture and training procedure as the one described by [22], with the only difference being the inputs and outputs. Moreover, we employ an improved label input (ILI) proposed by [21] for introducing time in the model, through conditional batch normalization [28]. A more comprehensive description of the time insertion in the CCGAN model, the architecture of the neural networks, the training procedure and speed-up may be found in [22]. The application of GANs for predicting the solution of partial differential equations is further detailed in [24, 25].

We define the geometry of our problems in Petrel [26]. A formation with dimensions 2000 m × 100 m × 100 m and discretized in a 401×1×100 uniformly distributed grid, thus mimicking a two-dimensional domain, is considered. We set one well injecting CO_2 at a supercritical state, in the center of the formation and fully connected with the formation. Additionally, we set two monitoring wells 500 m distant on both sides of the injection well. The geometry of our problem is illustrated in Fig. 2. The viscosity and density of the CO_2 are assumed to be 0.061 mPa·s and 733 kg/m³, respectively, whilst the viscosity and density of the brine are assumed to be 0.511 mPa·s and 1099 kg/m³, respectively. The CO_2 is injected for 10 years at a constant rate of $q_1 = 200$ m³/day. After that, the post-injection period begins when CO_2 is not injected anymore, lasting 20 additional years, giving 30 years of simulation in total.

We define 8 sets of parameters to generate correlated heterogeneous porosity distributions. In this case, considered parameters are: λ_x, λ_y and σ, and their different sets are presented in Table 1, together with the number of realizations for each of them. With Petrel [26] and the defined sets, we generate Gaussian distributed porosity fields with a mean value of 0.3, minimum of 0.15 and, maximum of 0.45. Petrel generates the Gaussian distribution with the specified mean and standard deviation and truncates it to satisfy the given minimum and maximum values.

We generate 13 realizations for each one of the sets C2, C4, C6 and C8, 27 realizations for C1 and C3, and 26 realizations for C5 and C7, for training the digital twin, totalling 158 realizations in the training data set. Since we are more interested in the predictions for highly heterogeneous formations, for testing, we generate 3 realizations for each set C1, C3, C5 and C7, and 1 realization for each C2, C4, C6 and C8, totalling 16 realizations in the testing data set.

Table 1. Sets of parameters for generating the heterogeneous porosity distributions, and the number of realizations for each one in the training and in the testing data sets.

Set	Parameters	Train samples	Test samples
C1	$\lambda_x = 100$ m, $\lambda_y = 10$ m, $\sigma = 1$	27	3
C2	$\lambda_x = 100$ m, $\lambda_y = 10$ m, $\sigma = 0.01$	13	1
C3	$\lambda_x = 100$ m, $\lambda_y = 2$ m, $\sigma = 1$	27	3
C4	$\lambda_x = 100$ m, $\lambda_y = 2$ m, $\sigma = 0.01$	13	1
C5	$\lambda_x = 500$ m, $\lambda_y = 10$ m, $\sigma = 1$	26	3
C6	$\lambda_x = 500$ m, $\lambda_y = 10$ m, $\sigma = 0.01$	13	1
C7	$\lambda_x = 500$ m, $\lambda_y = 50$ m, $\sigma = 1$	26	3
C8	$\lambda_x = 500$ m, $\lambda_y = 50$ m, $\sigma = 0.01$	13	1
	Total:	**158**	**16**

Given the generated porosity distributions, we derive permeability using a general model for carbonates proposed by [29, 30], that is:

$$\log(k) = (A - B\log(\text{rfn}) + [(C - D\log(\text{rfn}))\log(\phi)], \quad (5)$$

where $A = 9.7982$, $B = 12.0838$, $C = 8.6711$ and $D = 8.2965$ are constants, and rfn denotes the rock fabric number [31, 32], and is set to 3.5 throughout this work. Furthermore, log denotes the logarithm with base 10.

With the above-mentioned parameters, material properties, and boundary conditions, for the different realizations in the training and in the testing data sets, we simulate CO_2 injection using Eclipse [27]. We use timesteps of one-month-size, and the total simulation time, including initial state, is equal to 361 timesteps, *i.e.*, 30 years × 12 months + 1. For each porosity realization, we solve the transient CO_2 injection, which generates 57038 and 5776 data samples, respectively for training and testing the digital twin.

4. Results

In this section, we show the results for the prediction of the CO_2 plume motion with the CCGAN-based digital twin. The results in this paper were obtained via the usage of DCC resources [33], with the data generated being carried in an Intel® Xeon® Gold 6246R, and the training and testing of the CCGAN being in a NVIDIA® A100 80 GB.

As outlined in section 4, the CCGAN was trained with the 57038 data samples over 12 training states comprised of 5×10^4 steps each and tested with 5776 samples along the same training states. Our digital twin has the average pressure, the porosity and injection rate at the three wells as input, and the saturation distribution as output. Figure Fig. *3* shows examples of predictions of the CO_2 plume motion with the CCGAN, compared to the real saturation distributions. We randomly extracted these samples from the testing set, and the prediction here considers the last training state, *i.e.*, after 6×10^5 training steps.

We notice good approximations for the CO_2 saturation, given the limited input information of the model, and given that a mapping of an approximate CO_2 plume is retained. In addition, the CCGAN predictions follow the expected behavior of the CO_2 plume. During the injection of the CO_2, the plume spreads laterally according to the different heterogeneous porosity measured at the wells, as shown the lower panel of Fig. 3. As the injection ends, the plume stops propagating sidewards and ascends towards the impermeable cap-rock, as in the upper and mid panels of Fig. 3. We can also notice that the highest differences are at the edges of the plumes, where the transition zone for the CO_2 saturation is located.

For evaluating the accuracy of predicted outputs by the model, the relative error for each sample was calculated by

$$\text{rel. error} = \frac{\sum_{i=1}^{M} |O_i - \hat{O}_i|}{\sum_{i=1}^{M} |O_i|}, \tag{6}$$

in which O and $\hat{O}$ represent the output saturation given by Eclipse and by the CCGAN, respectively, and $M = 128 \times 128$ is the number of values in the output variable O for each time/realization, that is for each image. Figure Fig. 4 shows the box plot of relative errors for all samples in testing data every 5×10^4 training steps. We notice that at the very early stage of the training phase, *i.e.*, after 5×10^4 steps, the relative error ranges from 45% to 55%, but its median drops to around 5% in the second training state. With further training, the errors seem to reach a plateau with maximum of 10%, whilst no apparent over-fitting is observed. We consider this a reasonable accuracy, given that the input information is limited to the wells.

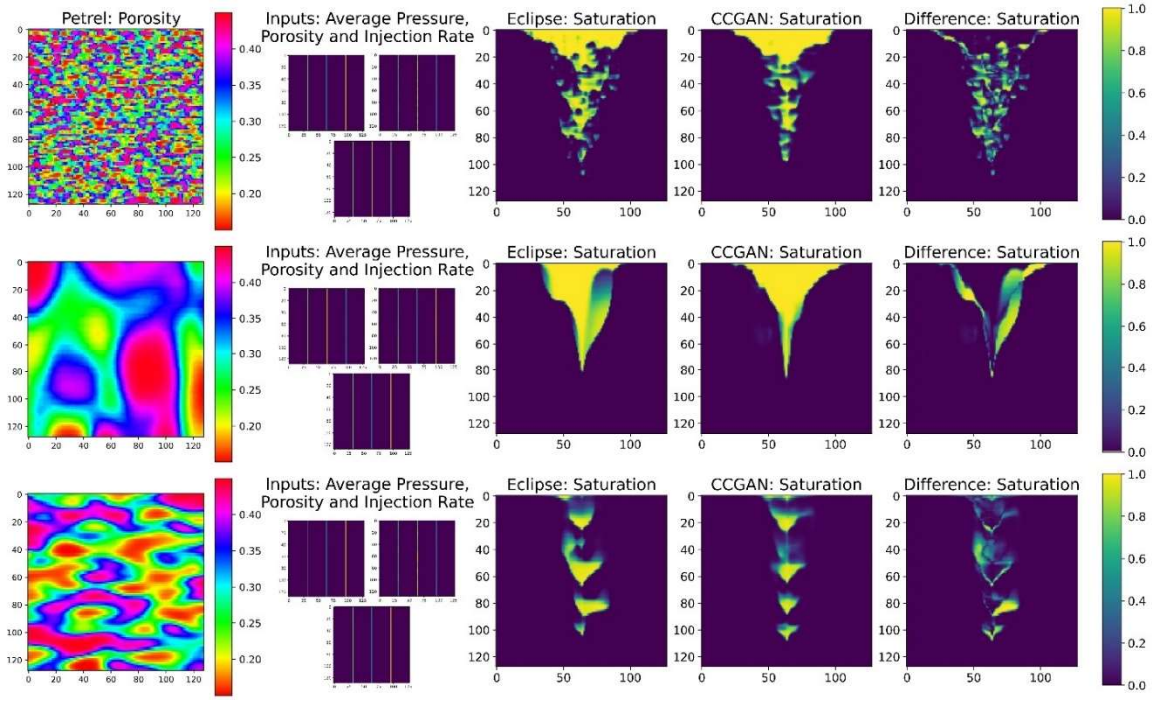

Fig. 3. Porosity distribution generated with Petrel, and comparison between the CO_2 saturation distribution obtained with Eclipse and the prediction with CCGAN.

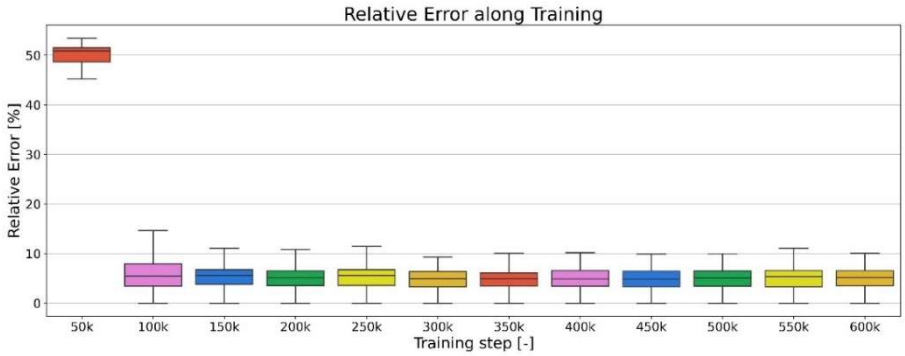

Fig. 4. Box plot of the relative error of the output saturation over the training steps. At an early stage of the training (50k-100k steps), the median of the error drops from around 51% to 5%. Additional training does not reflect any further decay in the errors, which are at most 10% in the last training state.

We illustrate in Fig. 5 how the relative error changes over time. We notice an increase in the error during the

injection period, followed by a smooth decay after the injection ends. This can be explained by the fact that the heterogeneous material properties, that represent the uncertainty for this model, have a high impact on the shape of the CO_2 plume during injection. In these early stages, the plume moves sidewards at a faster pace, driven by the pressure gradient generated by the injection. Conversely, after the injection ceases, the CO_2 plume ascends towards the impermeable cap-rock at a slower pace driven by buoyancy, thus being less impacted by the heterogeneity of the formation.

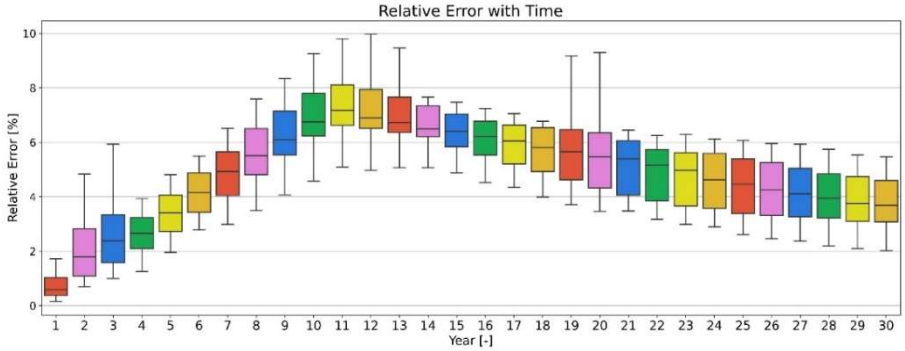

Fig. 5. Box plot of the relative error of the output saturation over the time. The errors increase during the injection period, *i.e.*, during the first 14 years, and decay after the injection ends.

5. Conclusion

In this work, we propose a novel technique for monitoring the CO_2 saturation plume motion during carbon storage practices. We developed a digital twin based on continuous conditional generative adversarial networks (CCGAN) that accurately predicts the CO_2 saturation given input data limited to the information available only at three wells.

This work's key findings are:

- The CCGAN-based digital twin predicts the CO_2 plume evolution with a minimum of 90% accuracy, which is quite reasonable given the limited input information and uncertainty in the formation material properties;
- The predicted plumes present the expected behavior of CO_2 plumes over time;
- A decrease in the accuracy of the model is observed during the injection phase, followed by increased accuracy after the injection ceases.

Our results suggest the potential application of a CCGAN-based digital twin for real-time monitoring of the CO_2 plume evolution due to the accuracy and speed of the predictions, given the limited information that is required as input for this model.

Acknowledgements

Carlos A. S. Ferreira, **Michal Stepien, Seyedbehzad Hosseinzadehsadati** and **Hamid M. Nick** and are supported by the Danish Offshore Technology Centre (DTU Offshore) and the research leading to the results in this paper has received funding from DTU Offshore under the Advanced Water Flooding program. Sandia National Laboratories is a multimission laboratory managed and operated by National Technology and Engineering Solutions of Sandia, LLC., a wholly owned subsidiary of Honeywell International, Inc., for the U.S. Department of Energy's National Nuclear Security Administration under contract DE-NA-0003525. This paper describes objective technical results and analysis. Any subjective views or opinions that might be expressed in the paper do not necessarily represent the views of the U.S. Department of Energy or the United States Government.

References

[1] C. R. Jenkins, P. J. Cook, J. Ennis-King, J. Undershultz, C. Boreham, T. Dance, P. de Caritat, D. M. Etheridge, B. M. Freifeld, A. Hortle, D. Kirste, L. Paterson, R. Pevzner, U. Schacht, S. Sharma, L. Stalker and M. Urosevic, "Safe storage and effective monitoring of CO2 in depleted gas fields," ConferenceProceedings of the National Academy of Sciences, vol. 109, no. 2, pp. E35-E41, 2012.

[2] T. Wildenborg, T. Leijnse, E. Kreft and Manuel Nepveu & Arie Obdam, "- Long-term safety assessment of CO2 storage: The scenario approach," E. S. Rubin, D. W. Keith, C. F. Gilboy, M. Wilson, T. Morris, J. Gale and K. Thambimuthu, Eds., Oxford, Elsevier Science Ltd, 2005, pp. 1283-1287.

[3] T. Mukerji, A. Jørstad, P. Avseth, G. Mavko and J. R. Granli, "Mapping lithofacies and pore-fluid probabilities in a North Sea reservoir: Seismic inversions and statistical rock physics," Geophysics, vol. 66, no. 4, pp. 988-1001, 2001.

[4] S. Lu and G. A. McMechan, "Estimation of gas hydrate and free gas saturation, concentration, and distribution from seismic data," Geophysics, vol. 67, no. 2, pp. 582-593, 2002.

[5] A. Pradhan and T. Mukerji, "Seismic Bayesian evidential learning: Estimation and uncertainty quantification of sub-resolution reservoir properties," Computational Geosciences, vol. 24, no. 3, pp. 1121-1140, 2020.

[6] T. M. Daley, J. B. Ajo-Franklin and C. Doughty, "Constraining the reservoir model of an injected CO2 plume with crosswell CASSM at the Frio-II brine pilot," International Journal of Greenhouse Gas Control, vol. 5, no. 4, pp. 1022-1030, 2011.

[7] M. W. Saaltink, V. Vilarrasa, F. De Gaspari, O. Silva, J. Carrera and T. S. Rötting, "A method for incorporating equilibrium chemical reactions into multiphase flow models for CO2 storage," Advances in Water Resources, vol. 62, pp. 431-441, 2013.

[8] M. Singh, A. Chaudhuri, M. R. Soltanian and P. H. Stauffer, "Coupled multiphase flow and transport simulation to model CO2 dissolution and local capillary trapping in permeability and capillary heterogeneous reservoir," International Journal of Greenhouse Gas Control, vol. 108, p. 103329, 2021.

[9] E. Houdu, O. Poupard and V. Meyer, "Supercritical CO2 leakage modelling for well integrity in geological storage project," in ConferenceProceedings of the COMSOL Conference 2008, 2008.

[10] B. Miyazaki, "Well integrity: An overlooked source of risk and liability for underground natural gas storage. Lessons learned from incidents in the USA," Geological Society, London, Special Publications, vol. 313, no. 1, pp. 163-172, 2009.

[11] A. Esposito and S. M. Benson, "Evaluation and development of options for remediation of CO2 leakage into groundwater aquifers from geologic carbon storage," International Journal of Greenhouse Gas Control, vol. 7, pp. 62-73, 2012.

[12] D. H. Bacon, N. P. Qafoku, Z. Dai, E. H. Keating and C. F. Brown, "Modeling the impact of carbon dioxide leakage into an unconfined, oxidizing carbonate aquifer," International Journal of Greenhouse Gas Control, vol. 44, pp. 290-299, 2016.

[13] Z. Zhong, A. Y. Sun and H. Jeong, "Predicting CO2 Plume Migration in Heterogeneous Formations Using Conditional Deep Convolutional Generative Adversarial Network," Water Resources Research, vol. 55, no. 7, pp. 5830-5851, 2019.

[14] Z. Wang, R. M. Dilmore and W. Harbert, "Inferring CO2 saturation from synthetic surface seismic and downhole monitoring data using machine learning for leakage detection at CO2 sequestration sites," International Journal of Greenhouse Gas Control, vol. 100, p. 103115, 2020.

[15] M. Liu and D. Grana, "Petrophysical characterization of deep saline aquifers for CO2 storage using ensemble smoother and deep convolutional autoencoder," Advances in Water Resources, vol. 142, p. 103634, 2020.

[16] H. Tang, P. Fu, C. S. Sherman, J. Zhang, X. Ju, F. Hamon, N. A. Azzolina, M. Burton-Kelly and J. P. Morris, "A deep learning-accelerated data assimilation and forecasting workflow for commercial-scale geologic carbon storage," International Journal of Greenhouse Gas Control, vol. 112, p. 103488, 2021.

[17] G. Wen, M. Tang and S. M. Benson, "Towards a predictor for CO2 plume migration using deep neural networks," International Journal of Greenhouse Gas Control, vol. 105, p. 103223, 2021.

[18] T. Kadeethum, F. Ballarin, Y. Choi, D. O'Malley, H. Yoon and N. Bouklas, "Non-intrusive reduced order modeling of natural convection in porous media using convolutional autoencoders: comparison with linear subspace techniques," Advances in Water Resources, vol. 160, p. 104098, 2022.

[19] F. Ballarin, A. D'amario, S. Perotto and G. Rozza, "A POD-selective inverse distance weighting method for fast parametrized shape morphing," International Journal for Numerical Methods in Engineering, vol. 117, no. 8, pp. 860-884, 2019.

[20] J. Hesthaven, G. Rozza and B. Stamm, Certified reduced basis methods for parametrized partial differential equations, Springer, 2016.

[21] X. Ding, Y. Wang, Z. Xu, W. J. Welch and Z. J. Wang, "Continuous Conditional Generative Adversarial Networks: Novel Empirical Losses and Label Input Mechanisms," arXiv preprint arXiv:2011.07466, 2020.

[22] T. Kadeethum, D. O'Malley, Y. Choi, H. S. Viswanathan, N. Bouklas and H. Yoon, "Continuous conditional generative adversarial networks for data-driven solutions of poroelasticity with heterogeneous material properties," arXiv preprint arXiv:2111.14984, 2021.

[23] M. Mirza and S. Osindero, "Conditional generative adversarial nets," arXiv:1411.1784, 2014.

[24] T. Kadeethum, D. O'Malley, J. N. Fuhg, Y. Choi, J. Lee, H. S. Viswanathan and N. Bouklas, "A framework for data-driven solution and parameter estimation of PDEs using conditional generative adversarial networks," Nature Computational Science, vol. 1, no. 12, pp. 819-829, 2021.

[25] C. A. Ferreira, T. Kadeethum, N. Bouklas and H. M. Nick, "A framework for upscaling and modelling fluid flow for discrete fractures using conditional generative adversarial networks," Advances in Water Resources, vol. 166, p. 104264, 2022.

[26] Schlumberger, Petrel, Release 2021.3, 2021.

[27] Schlumberger, Eclipse, Release 2021.4, 2021.

[28] H. De Vries, F. Strub, J. Mary, H. Larochelle, O. Pietquin and A. C. Courville, "Modulating early visual processing by language," Advances in Neural Information Processing Systems, vol. 30, 2017.

[29] F. J. Lucia, J. W. Jennings Jr, M. Rahnis and F. O. Meyer, "Permeability and rock fabric from wireline logs, Arab-D reservoir, Ghawar field, Saudi Arabia," GeoArabia, vol. 6, no. 4, pp. 619-646, 2001.

[30] J. W. Jennings and F. J. Lucia, "Predicting permeability from well logs in carbonates with a link to geology for interwell permeability mapping," SPE Reservoir Evaluation & Engineering, vol. 6, no. 04, pp. 215-225, 2003.

[31] F. J. Lucia, "Petrophysical parameters estimated from visual descriptions of carbonate rocks: a field classification of carbonate pore space," Journal of petroleum technology, vol. 35, no. 03, pp. 629-637, 1983.

[32] F. J. Lucia, "Rock-fabric/petrophysical classification of carbonate pore space for reservoir characterization," AAPG bulletin, vol. 79, no. 9, pp. 1275-1300, 1995.

[33] DTU Computing Center, DTU Computing Center resources, Technical University of Denmark, 2021.